

AMER.96.009

Code 500.90.400 Project GRB406 (76224)

(General Research)

Fracture mechanics: Prediction of cleavage fracture in
the brittle to ductile transition region of a ferritic steel

by

R.W.J. Koers

CONFIDENTIAL

This is a CONFIDENTIAL document. Any distribution beyond the parties listed within must be authorized by Shell International Oil Products B.V. Reference to this document should only be made in documents having the same, or a higher, security classification.

Copyright is vested in Shell International Oil Products B.V., The Hague.

Neither the whole nor any part of this document may be reproduced, stored in any retrieval system or transmitted in any form or by any means (electronic, mechanical, reprographic, recording or otherwise) without the prior written consent of the copyright owner.

AMER.96.009

Code 500.90.400 Project GRB406 (76224)

(General Research)

Fracture mechanics: Prediction of cleavage fracture in
the brittle to ductile transition region of a ferritic steel

by

R.W.J. Koers

Approved by:

P. Bristol

Keywords: fit for purpose, ductile fracture, cleavage fracture, micro-mechanics, Gurson model, damage, finite elements, Fe510 steel, miniature fracture mechanics tests

Executive Summary

Fracture mechanics approaches are currently applied to perform defect assessments of Group's equipment, which either contain fabrication defects or have degraded during service with resultant defect extension. The results of such assessments lead to inspection criteria, strategies, recommendations to limit risk of failure and lifetime predictions extensions etc.

In spite of the general applicability of fracture mechanics it still has significant shortcomings in that it can be overconservative and has limited predictive capabilities. Examples of limitations are the inability to predict both thickness effects on fracture and the shape of the brittle-ductile fracture transition curve. The development of local approach methods as described in this report give the opportunity for overcoming some of these shortcomings and also realising applications of great practical significance. An example has been the application of such methods for MF in deciding on temperatures to hydrotest pressure vessels when there is very limited materials information. The approach described is a development of previous work at Billiton Research B.V., Arnhem (BRA). A new method has been developed to predict whether cleavage fracture will still occur after initiation of ductile crack growth. This is important because now the relevance and significance of such phenomenon can be more rationally judged. Further research is required to improve the model's accuracy and applicability. There is also a practical spin-off of the work in the development of test specimens which require minimal amounts of material. This is needed in fitness for purpose analyses where material is rarely available in sufficient quantities for the normal fracture mechanics testing.

AMER.96.009

Code 500.90.400 Project GRB406 (76224)

(General Research)

Fracture mechanics: Prediction of cleavage fracture in
the brittle to ductile transition region of a ferritic steel

by

R.W.J. Koers

Approved by:

P. Bristol

Keywords: fit for purpose, ductile fracture, cleavage fracture, micro-mechanics, Gurson model, damage, finite elements, Fe510 steel, miniature fracture mechanics tests

Technical Summary

A model is presented to predict the event of cleavage fracture in the brittle to ductile transition region. In this region cleavage fracture could occur after some amount of ductile tearing. The model takes into account the competition between the nucleation of voids at second phase inclusions leading to ductile fracture and the nucleation of unstable micro cracks initiated at second phase inclusions leading to cleavage fracture. The model was tested on four point bend specimens of a ferritic steel tested in the brittle to ductile transition region. It was shown that there could be a significant amount of ductile crack growth before the specimens failed by cleavage. Two different crack growth simulations were performed to investigate the stresses ahead of a ductile growing crack. One simulation takes into account the softening of the material in the process zone, due to damage, around a quasistatically ductile growing crack. The second simulation neglects this damage. It was found that the crack opening stress near the crack tip in the process zone is significantly lower than in the analysis neglecting the effect of damage. Further from the crack tip, outside the damage zone the crack opening stresses are similar in both simulations.

Contents

	Page
1. Introduction	1
2. Material	1
3. Cleavage fracture model	1
4. Experiments	2
5. The transition of ductile tearing into cleavage fracture	3
6. Crack growth simulation using the von Mises yield criterion	3
6.1 Simulation experimental fracture resistance curve	3
6.2 Calculated stress distribution and prediction of cleavage fracture	4
7. Crack growth simulation using the modified Gurson damage model	5
7.1 Modified Gurson model	5
7.2 Calculated fracture resistance curves	7
7.3 Calculated stress distribution	8
8. Model to describe cleavage fracture in the brittle to ductile transition region	8
8.1 Model description	8
8.2 Prediction of cleavage fracture after some amount of ductile tearing	9
9. Discussion	9
10. Conclusions and recommendations	9
Figure 1 Material true-stress versus true-strain curve at -40 °C	10
Figure 2 Fracture resistance curve of a Fe510 steel measured on side grooved 4-point single edge notched bend specimens tested at -40 °C	10
Figure 3 Calculated load versus load line displacement as a function of crack length for the Fe510 steel 4SENB specimen tested at -40 °C	11

Contents (Cont'd)

	Page	
Figure 4	Calculated constant load line displacement curves ($\Delta_L = 1.0, 1.4, \dots, 4.2, 4.6$ mm) as a function of J and Δa with the measured fracture resistance curve	12
Figure 5	Node relaxation technique	12
Figure 6	Calculated stress distribution ahead of the growing crack in the 4SENB specimen based on the von Mises flow criterion	13
Figure 7	Calculated probability of cleavage fracture and calculated resistance curve based on the von Mises flow criterion	13
Figure 8	Damage analyses: Calculated fracture resistance curve and experimental data	14
Figure 9	Damage analyses: Calculated load versus CMOD curves and experimental data	14
Figure 10	Damage analysis: Calculated crack opening stress ahead of the crack tip as a function of the amount of crack growth	15
Figure 11	Damage analyses: Predicted cleavage fracture probability as a function of the prior amount of ductile tearing	15
Appendix I	Implementation modified Gurson model in the MARC finite element package	
References		

1. Introduction

Within the first phase of an International Collaborative Fracture Programme [1], various cracked geometries of a ferritic structural steel were tested in the brittle-ductile transition temperature region, and analysed by common safety assessment methods based on the critical crack opening displacement (CTOD) and the critical J integral. The accuracy of such predictions is limited by the large scatter in measured values of these critical, single parameter fracture mechanics parameters in this temperature region.

To describe the large scatter of cleavage fracture at the lower end of the brittle-ductile transition region a statistical approach was used [2]. Good results were obtained for the predictions of cleavage fracture initiation, for both three-point single edge notched and four-point single edge notched specimens with a pre-fatigue crack and a wide plate with two pre-fatigue cracks. However, for the specimens which failed by cleavage after more than 0.2 mm ductile tearing, the measured fracture toughness values were significantly higher than those predicted. In [2] the predictions were based on finite element analysis of the geometries tested. A constant crack length was assumed and crack growth was neglected.

To study the transition of ductile tearing into cleavage fracture, the ductile crack growth process has been simulated using finite elements. Two different types of finite element crack growth simulations were performed. The first one is a simulation of the crack growth process using classical theory of plasticity with a node release technique and the second uses the modified Gurson damage model. The calculated transient stress/strain distributions ahead of the growing crack were used in combination with the statistical cleavage fracture model to predict the event of cleavage fracture after some amount of ductile tearing.

2. Material

The material used in this study is a ferritic C-Mn steel with designation Fe510Nb of quality Fe 355-KT according to Euronorm 113-72. The true stress versus true strain curve measured on smooth round tensile specimens, is shown in Figure 1. The tensile tests were performed at -40 °C, the temperature of the fracture mechanics tests. The true strain was measured from the diameter reduction at the necking region in the tensile tests. True stress was estimated from the load and the diameter reduction and was corrected for the tri-axial stress state in the necking according to the Bridgeman type of procedure, as proposed by Bakker [3].

3. Cleavage fracture model

In ferritic steels, cleavage fracture usually occurs by unstable micro cracks initiated at brittle second phase inclusions. Due to the scatter in such factors as size, orientation and shape of such inclusions, and the non-uniform stress field around a loaded crack tip, the event of cleavage fracture has a statistical nature. A weakest link model [4, 5] was used by BAKKER and KOERS [2] to predict cleavage fracture initiation of three and four point single edge notched fracture mechanics specimens and a wide plate geometry. Both a two and three parameter Weibull model were proposed. In the two-parameter Weibull model it was assumed that cleavage fracture could occur by the onset of plastic deformation, and in the three-parameter Weibull model a threshold stress has been assumed in addition. If the occurrence of plasticity is taken as the lower bound, it would mean that for a temperature far above the brittle to ductile transition region there is still a probability of cleavage fracture. A three-parameter Weibull model on the other hand where the lower bound is defined by a threshold of the maximum normal stress, would avoid this unrealistic outcome because a sufficiently high threshold stress would not allow cleavage fracture at higher temperature.

The stress ahead of a loaded crack tip decreases with increasing temperature due to the lowering of stress strain curves at higher temperatures.

The cumulative probability of cleavage fracture, P_f was defined as follows:

Two parameter Weibull model:

$$P_f = 1 - \exp \left[- \left(\frac{\sigma_w}{\sigma_u} \right)^m \right] \quad (1)$$

where the Weibull stress, σ_w , is defined as

$$\sigma_w = \left(\int_{V_{pl}} \sigma(\mathbf{x})^m \frac{dV}{V_o} \right)^{1/m} \quad \text{with } V_{pl} \in V \text{ where } \varepsilon_{pl} > 0, \quad (2)$$

V_{pl} is the plastic part of volume V , V_o is a reference volume taken as 1 mm^3 and $\sigma(\mathbf{x})$ is the maximum normal stress at material point $\mathbf{x} = (x, y, z)^T$. The Weibull parameters m and σ_u were determined from finite element analyses of notched round bar tensile tests at $-170 \text{ }^\circ\text{C}$. The parameter m describing the scatter of the maximum normal stress at which reference volume V_o failed was found to be 27.2 and the σ_u is the characteristic (63.2 percent value) of the distribution was found to be 1542 MPa.

Three-parameter Weibull model:

$$P_f = 1 - \exp \left[- \left(\frac{\sigma_w - \sigma_{th}}{\sigma_u} \right)^m \right] \quad \text{for } \sigma_w \geq \sigma_{th} \quad (3)$$

where the Weibull stress, σ_w , is now defined as

$$\sigma_w = \sigma_{th} + \left(\int_{V_{th}} (\sigma(\mathbf{x}) - \sigma_{th})^m \frac{dV}{V_o} \right)^{1/m} \quad \text{with } V_{th} \in V \text{ where } \sigma(\mathbf{x}) \geq \sigma_{th} \wedge \varepsilon_{pl} > 0 \quad (4)$$

and σ_{th} is the threshold stress. The parameters for the three-parameter Weibull model were determined as $m = 1.0$, $\sigma_u = 221 \text{ MPa}$ and $\sigma_{th} = 1375 \text{ MPa}$.

4. Experiments

To investigate the transition of ductile fracture into a mechanism of cleavage fracture a series of fifteen fracture mechanics specimens were fractured at $-40 \text{ }^\circ\text{C}$, which is in the middle of the brittle to ductile temperature transition region for the Fe510 steel considered. All specimens failed by cleavage after some ductile tearing. Large scatter was observed in the measured fracture toughnesses. However when the fracture toughness points are plotted as a function of initial ductile crack growth, the points fall on one line representing the ductile fracture resistance curve of the material, Figure 2. The specimens tested were four point single edge notched bend specimens (4SENB). The width W and the thickness B were 30 mm. The relative crack depth a/W was 0.3. The specimens had 20% side grooves, net section thickness $B_N = 24 \text{ mm}$, in order to approach a plane strain condition along the whole crack front.

5. The transition of ductile tearing into cleavage fracture

At low temperature cleavage fracture was assumed to be characterised by the unstable propagation of micro cracks initiated at brittle carbide particles. While at higher temperatures ductile fracture is characterised by void nucleation associated with non-metallic inclusions and carbides. In the transition region there is a competition between both the cleavage and the ductile fracture mechanism, see e.g.[6].

In the two-parameter Weibull model the lower bound of the cleavage fracture stress has been determined by the onset of plasticity. For the three-parameter Weibull model a threshold stress has been assumed as a lower bound and was determined to be significantly higher than the maximum normal stress determined by the onset of plasticity. Justification for the threshold is that at higher temperatures at the upper shelf of the brittle to ductile transition curve no cleavage fracture occurs. The explanation is that the stress strain curve decreases with increasing temperature, which results in decreasing maximum normal stress ahead of the crack tip with increasing temperature. Therefore, in the transition region there is a temperature at which the maximum normal stress ahead of the crack tip marginally reaches the required cleavage fracture stress. Ductile tearing can then be initiated. The ductile tearing has been observed after some crack growth to suddenly transform into a fast cleavage fracture. No single explanation can be given for this change in mechanism, a combination of different causes seems to be most plausible. Possible causes are:

- The stress field ahead of a ductile growing crack changes from the stress field for a constant crack length to a stress field with a higher constraint resulting in higher stresses for a growing crack.
- The volume, with a high maximum normal stress, sampled increases as the crack extends. This results, according to the Weibull models, in an increasing probability of cleavage fracture.

Finite element crack growth analyses have been performed to investigate the transition of ductile tearing into cleavage fracture. The calculated transient stress field ahead of the ductile growing crack is used to calculate the Weibull stress and its corresponding probability of cleavage fracture as a function of ductile crack growth. Two different types of finite element analyses were performed to calculate the transient stress field ahead of the ductile growing crack. The first analysis is a simulation of the ductile fracture process using the von Mises yield criterion and the measured fracture resistance curve as input. The second analysis is based on the modified Gurson damage model for ductile fracture.

6. Crack growth simulation using the von Mises yield criterion

6.1 Simulation experimental fracture resistance curve

The measured fracture resistance curve, Figure 2, has been used to determine the boundary condition, the load line displacement (Δ_L) versus crack growth relation that needs to be applied in the crack growth simulation. The procedure to derive the load line displacement versus crack growth relation that was applied in the crack growth simulations was the following. A series of 11 two dimensional, plane strain, elastic-plastic finite element analyses were performed on a 4SENB specimen with crack lengths varying from $a = 9.0$ mm to $a = 11.0$ mm with steps of 0.2 mm. From the results of these analyses a crack driving force diagram with lines of constant load-line displacements was constructed with the axes J and the amount of crack growth Δa respectively. The initial crack length was taken as 9.0 mm. The required Δ_L versus Δa relation can be derived by drawing the measured fracture resistance curve onto this diagram. The use of a plane strain assumption is only correct in the close vicinity of the crack tip. However, the material volume that contributes to the cleavage fracture probability is also limited to a small region around the crack tip which is actually plane strain.

The calculated load versus Δ_L curves for crack lengths varying from 9.0 mm to 11.0 mm are given in Figure 3. From these curves the J integral as a function of applied Δ_L has been calculated for each crack length. A crack driving force diagram with lines of constant load line displacements as a function of crack growth Δa , for an initial crack length of 9.0 mm, has been derived from these results and is shown in Figure 3. The measured fracture resistance curve is also plotted in Figure 3. Initiation is assumed at the intersection between the 0.2 mm offset blunting line and the fracture resistance regression line, see Figure 2. This results in a J initiation value equal to 182 N/mm. The derived crack growth versus applied load line displacement relations is:

$$\Delta_L = 2.542 (\Delta a + 0.405)^{0.644} \quad (5)$$

The derived load line displacement versus crack growth relations, Eq. 5, was prescribed in the finite element crack growth simulation to calculate the transient stress-strain distribution around a ductile growing crack. Because of symmetry only one half of the 4SENB specimen had to be modelled. The finite element mesh contained 3531 nodes and 3413 four-node isoparametric quadrangular plane strain elements. The initial crack tip was modelled by a small circle with a radius of 0.01 mm in order to avoid the need of singular elements at the start of the computation and to be able to calculate the stress/strain field accurately until initiation. The length of the finite elements used along the crack path is equal to 0.02 mm. Such a fine mesh in combination with finite strains and displacement effects, which were included in the analysis by applying an updated Lagrange procedure, have been used in order to obtain the best possible estimates of the stress distribution near the growing crack.

Crack growth is modelled by means of the node relaxation technique [7], which consists of the following steps (see Figure 3):

- (a) At the moment the crack tip position passes an element border, the boundary condition at point 1 is removed. In addition an external force is applied equal to the reaction force at the instant the crack tip reached point 1;
- (b) The external force is then assumed to decay in a given number of increments until the crack tip location reaches the next element. In the analyses presented the decay of the external force was done in 20 equal steps.

The external force at the corner node (point 1) is released in the following manner:

$$F_i = F_o \left[1 - \frac{\delta_i}{d} \right] \quad (6)$$

where d is the element length, δ_i the amount of crack propagation along the element, F_o the reaction force acting at the corner node at the time instant the crack reaches the corner node and F_i the force acting at the corner node at step i . The above node relaxation process was automated such that no user interference is required during the crack growth simulation.

6.2 Calculated stress distribution and prediction of cleavage fracture

The calculated crack opening stress distributions ahead of the growing crack as a function of the amount of crack growth are given in Figure 3. The calculated true plastic strain ahead of the crack tip was approximately 100 %, therefore no extrapolation of the measured stress strain curve was necessary during the analysis. The Weibull stress and the corresponding probability of cleavage fracture were calculated from the calculated stress distributions ahead of the growing crack for both the two-parameter and the three-parameter Weibull model. Both the calculated probability of cleavage fracture as a function of applied J and the calculated fracture resistance curve are given in Figure 0. The calculated resistance curve in Figure 0 is in good agreement, as expected, with the resistance curve of Figure 3 used as input for the crack growth simulation. However, from the calculated probability of cleavage fracture, cleavage fracture is expected to occur before initiation of ductile tearing or after a

small amount ($\Delta a < 0.2$ mm) of ductile tearing. Cleavage fracture occurred in the experiments after significant ductile tearing in the range from $\Delta a = 0.5$ -2.8 mm. A possible reason for predicting cleavage fracture too soon is the calculated rapidly increasing level of stress in the process zone around the tip of the quasistatically growing crack. The distribution of the crack opening stresses ahead of the growing crack does change from that known for a stationary crack [8] to one of a singular nature. A similar tendency of the crack opening stress was found by VARIAS and SHIH [9]. The values of the calculated stresses in the element nearest by the growing crack tip would have been lower when a mesh with larger elements would have been chosen. Although, with the von Mises yield criterion and a very fine mesh as used in this analysis the best estimate of the analytical stress distribution of a growing crack is obtained, independently from the question whether a physical process has been modelled. In reality such high stresses do not exist in the process zone due to damage of the material. Since the cleavage fracture predictions are sensitive to the accuracy of the calculated maximum principal stresses, the used analysis method is unreliable for cleavage fracture predictions after some amount of crack growth. Therefore the predictions were extended using a damage model to take into account the softening of the material in the process zone around a crack tip.

7. Crack growth simulation using the modified Gurson damage model

7.1 Modified Gurson model

Based on the work of BERG [10], which show that a porous medium is governed by the normality rule if the matrix material follows this rule, GURSON [11, 12] derived approximate yield functions for materials containing either cylindrical or spherical voids. In the case of spherical voids, with a volume fraction f , the approximate yield function is given by:

$$\Phi = \frac{\sigma_e^2}{\sigma_M^2} + 2 q_1 f^* \cosh\left(\frac{q_2 \sigma_{kk}}{2 \sigma_M}\right) - \{1 + (q_1 f^*)^2\} = 0 \quad (7)$$

In Eq. 7, $\sigma_e = (\frac{3}{2} s_{ij} s_{ij})^{1/2}$ is the macroscopic effective stress and $s_{ij} = \sigma_{ij} - \frac{1}{3} \sigma_{kk} \delta_{ij}$ represents the stress deviator. The actual microscopic stress state in the matrix material is represented by an equivalent flow stress σ_M . When $f^* \equiv 0$ Eq. 7 reduces to the von Mises flow criterion.

The parameters q_1 and q_2 were introduced by TVERGAARD [13] to bring predictions of the Gurson model at low volume fractions into closer agreement with full numerical analysis for periodic arrays of voids. With f^* equal to f and $q_1 = q_2 = 1.0$, Eq. 7 reduces to the function as originally proposed by Gurson. The function $f^*(f)$ was introduced by TVERGAARD and NEEDLEMAN [14] to model the more rapid loss of material stress carrying capacity associated with coalescence of voids.

$$\begin{aligned} f^*(f) &= f && \text{if } f \leq f_c \\ &= f_c + \frac{f_u - f_c}{f_F - f_c} (f - f_c) && \text{if } f > f_c \end{aligned} \quad (8)$$

so that the modification $f^*(f)$ becomes active when the void volume fraction f exceeds a critical value f_c , and complete loss of stress carrying capacity (coalescence of voids) occurs when $f = f_F$ so that $f_u^* = f^*(f_F) = 1/q_1$.

The microscopic equivalent flow stress σ_M and the equivalent plastic strain ϵ_M^p are averages which do not specify the actual microscopic fields in the matrix material surrounding the voids. However, it is assumed that the rate of equivalent plastic work in the matrix material equals the macroscopic rate of plastic work,

$$\sigma_{ij} \dot{\epsilon}_{ij}^p = (1 - f) \sigma_M \dot{\epsilon}_M^p. \quad (9)$$

The plastic part of the macroscopic strain rate, $\dot{\epsilon}_{ij}^p$, is taken in a direction normal to the flow criterion and is given by:

$$\dot{\epsilon}_{ij}^p = \Lambda \frac{\partial \Phi}{\partial \sigma_{ij}}. \quad (10)$$

Combining Eqs. 9 and 10 results in the following expression for the proportionality factor, Λ :

$$\Lambda = \frac{(1 - f) \sigma_M \dot{\epsilon}_M^p}{\sigma_{ij} \frac{\partial \Phi}{\partial \sigma_{ij}}}. \quad (11)$$

The rate of change of the void volume fraction results from void nucleation as well as from growth of existing voids.

$$\dot{f} = \dot{f}_{growth} + \dot{f}_{nucleation}. \quad (12)$$

The void growth rate of existing voids is determined from the condition of plastic incompressibility of the matrix material,

$$\dot{f} = (1 - f) \dot{\epsilon}_{kk}^p \quad (13)$$

where $\dot{\epsilon}_{kk}^p$ represents the macroscopic plastic strain rate.

Two different nucleation criteria were considered, a stress controlled nucleation criterion and a strain controlled nucleation criterion. Due to the interaction effects between particles and the scatter in e.g. particle spacing, size and shape, statistical distributions were used to describe the nucleation of voids as proposed by CHU and NEEDLEMAN [15]. Assuming that nucleation only depends on the stress transmitted across the particle-matrix interface they adopted the idealisation that there is a mean critical stress for nucleation, σ_N , and that the nucleation stress is normally distributed. We will employ the sum of the matrix flow stress, σ_M , and the hydrostatic stress as a measure of the maximum stress at the interface [16]. The stress controlled nucleation criterion is then given by:

$$\dot{f}_{nucleation} = \left(\dot{\sigma}_M + \frac{\dot{\sigma}_{kk}}{3} \right) \frac{f_N}{s_\sigma \sqrt{2\pi}} \exp \left[-\frac{1}{2} \left\{ \frac{\left(\sigma_M + \frac{\sigma_{kk}}{3} \right) - \sigma_N}{s_\sigma} \right\}^2 \right] \quad (14)$$

where f_N is the volume fraction of the void nucleating particles and s_σ the standard deviation of the stress over which most of the voids nucleate.

However as pointed out by GOODS and BROWN [17] it is important to realise that this criterion is derived on the basis of a critical stress at the interface of the particle, and as this stress is produced by the local work hardening at the particle, it is therefore a function of the plastic strain in the matrix material so the failure criterion refers fundamentally to strain. Therefore a similar idealisation as Eq. 14 can be made for the mean equivalent plastic strain, ϵ_N^P , at which nucleation occurs. The *strain* controlled nucleation criterion is then given by:

$$\dot{f}_{nucleation} = \dot{\epsilon}_M^P \frac{f_N}{s_\epsilon \sqrt{2\pi}} \exp \left[-\frac{1}{2} \left(\frac{\epsilon_M^P - \epsilon_N}{s_\epsilon} \right)^2 \right] \quad (15)$$

where s_ϵ is the standard deviation of the equivalent plastic strain and ϵ_M^P the equivalent plastic strain of the matrix material.

Together with the nucleation criteria the whole process of void nucleation, void growth and coalescence is accounted for by the modified Gurson model and was used as the basis for the ductile crack growth damage analyses within this study. The model was implemented in the MARC [18] finite element package.

7.2 Calculated fracture resistance curves

The modified Gurson model was used to simulate the process of ductile tearing. Stress controlled nucleation has been assumed with a mean critical stress for nucleation of three times the yield stress, $\sigma_N = 3 \sigma_{yield}$, and the standard deviation $s_\sigma = 0.5 \sigma_{yield}$. Image analysis was used at BRA to measure the void volume fraction of void nucleating particles and was taken as $f_N = 0.001$. Cell studies performed by KOPLIK and NEEDLEMAN [19] indicated that the critical void volume fraction f_c depends mainly on the initial void volume fraction. This paper was used as a guidance on the choice of parameters. For an initial void volume fraction equal to 0.001, the critical volume fraction $f_c = 0.03$. The parameter f_F was taken as 0.15 and the parameter $q_1 = 1.25$. The resistance curve derived from an analysis performed with q_2 equal to 1.0 was too flat. To get a steeper slope for the fracture resistance curve, q_2 was set equal to 0.98. A lower value of q_2 reduces the contribution of the hydrostatic stress on void growth resulting in a steeper resistance curve. Crack initiation is assumed when the first element ahead of the original crack tip has failed and the amount of crack growth is defined by the accumulated length of the failed elements (in the undeformed geometry).

Ahead of the crack tip square finite elements with a length of 0.1 mm have been used. The size of the finite elements were chosen to get reasonable agreement with initiation. It was found that the level of the resistance curve is strongly influenced by the chosen finite element size. Approximately, doubling the size of the finite elements resulted in a doubling of the calculated J integral at initiation and dividing the finite elements into halves resulted in half of the calculated J integral values.

The calculated fracture resistance curve is given in Figure 3. The result is in reasonable agreement with the experimental data. However comparing the calculated applied load versus Crack Mouth Opening Displacement (CMOD) relationship with the experimental data, see Figure 3, it can be concluded that the fit is not yet optimal. The calculated load versus CMOD response is too stiff in the early stage, until crack initiation, due to the assumed plane strain condition and is lower than the experimental data during crack growth. A further detailed sensitivity analysis is required to improve this. To be able to compare the experimental data with the calculations, the applied load was normalised as follows

$$P_N = \frac{PW}{(W - a_0)^2 B_N \sigma_{yield}} \quad (16)$$

where P_N is the normalised load, P is the applied load, W the specimen width, a_0 the initial crack length, B_N the net thickness which is in our case 80 % of the specimen thickness.

7.3 Calculated stress distribution

The calculated crack opening stresses ahead of the quasistatically growing crack are given in Figure 3. The stresses near the crack tip in the process zone are significantly lower than those determined without damage, see Figure 3. This is due to the softening behaviour of the material due to the damage. Further away from the crack tip outside the process zone the calculated stresses are of the same order for both the analyses with and without damage.

8. Model to describe cleavage fracture in the brittle to ductile transition region

8.1 Model description

Within the cleavage fracture model it was assumed that cleavage fracture occurs by unstable micro cracks initiated at brittle second phase inclusions. A two-parameter Weibull model and a three-parameter Weibull model were used to take into account the statistical nature of cleavage fracture. On the other hand, ductile crack tearing was described by the mechanism of growth of voids and coalescence of these voids nucleated at second phase inclusions. Void nucleation was described by a stress controlled nucleation criterion. For cleavage fracture, after some ductile tearing the nucleation criteria for cleavage and ductile fracture are competitive. Once a void has been nucleated at an inclusion, that inclusion cannot contribute to the mechanism of cleavage fracture. A modification of the cleavage fracture models as given in Eqs. 1- 4 is proposed to take this phenomena into account.

With reference to [2] it is assumed, for the two-parameter Weibull model without void nucleation, that the cleavage probability P_f of a reference volume V_0 stressed by a maximum normal stress σ is given by:

$$P_f(V_0; \sigma) = 1 - \exp\left[-\left(\frac{\sigma}{\sigma_u}\right)^m\right] \quad (17)$$

where m is the Weibull parameter, σ_u is the characteristic (63.2 %) value of the distribution. When nucleation of voids could also occur, the probability of cleavage fracture for reference volume V_0 could be defined as:

$$P_f(V_0; \sigma) = 1 - (1 - P_{void\ nucleation}) \exp\left[-\left(\frac{\sigma}{\sigma_u}\right)^m\right] \quad (18)$$

where $P_{void\ nucleation}$ is the probability of void nucleation in V_0 . Since cleavage fracture is always preceded by some amount of plastic deformation only the plastically deformed part, V_{pl} , of the total volume of a component has to be taken into account. Cleavage fracture is assumed to be triggered by a micro-crack most critically loaded in V_{pl} resulting in an unstable crack propagation. Dividing V_{pl} into n reference volumes V_0 , $V_{pl} = n V_0$, results in the following probability of cleavage fracture of a loaded component

$$P_f(V_{pl}; \sigma) = 1 - \prod_{i=1}^n (1 - P_{void\ nucleation_i}) \exp \left[- \left(\frac{\sigma_i}{\sigma_u} \right)^m \right] \quad (19)$$

where index i stands for the i -th reference volume element. When the probability of void nucleation is zero then Eq. 19 results in the two-parameter Weibull model as defined in Eq. 1. A similar approach was followed for the three-parameter Weibull model.

8.2 Prediction of cleavage fracture after some amount of ductile tearing

The model to describe cleavage fracture after some amount of ductile tearing was used to predict cleavage fracture of the 4SENB specimens. The crack growth simulation performed with the modified Gurson model has been used as input for the cleavage fracture analysis. To be able to apply the cleavage fracture model the probability of void nucleation is required as a function of loading at each material point in the finite element mesh. The probability of void nucleation of a material point was determined from the stresses calculated using the cumulative probability of Eq. 14. The calculated probability of cleavage fracture as a function of the amount of ductile crack growth, together with the rank probability of the experimental data, is given in Figure 3. A significant improvement has been obtained compared with the results where damage is neglected, see Figure 0. Although the predictions are conservative, cleavage is still predicted too soon. A more detailed investigation is required to determine the sensitivity of the different Gurson model parameters on the calculated resistance curve and the predicted probability of cleavage fracture.

9. Discussion

In the analyses performed with the modified Gurson model it was found that the finite element size has a strong influence on predicted fracture resistance curves. The calculated J integral at initiation values vary approximately linearly with chosen finite element size. This will be addressed in a forthcoming report, but does not affect the outcome of this study.

The apparent complexity of the method and material input requirements will be addressed in a future report where it will be shown that this can be overcome.

This study is also related to another study being carried out at BRA using a decohesion model for predicting ductile crack growth. This latter model is dedicated to the ductile failure mode and does not address the problem of fracture mode transition behaviour.

10. Conclusions and recommendations

The stresses near the crack tip in the process zone of a quasistatically growing crack taking into account the development of ductile damage, are significantly lower than those determined without taking damage into account. However further away from the crack tip, outside the process zone, the calculated stresses are in the same order for both the analyses with and without damage.

A model to predict cleavage fracture in the ductile to brittle transition region is presented. The model takes into account the competition between the nucleation criteria for cleavage fracture and for ductile fracture. The results obtained are promising. However a more detailed sensitivity analysis is required to determine the effect of the assumed nucleation stress and other parameters.

Amsterdam, June 1996

vg

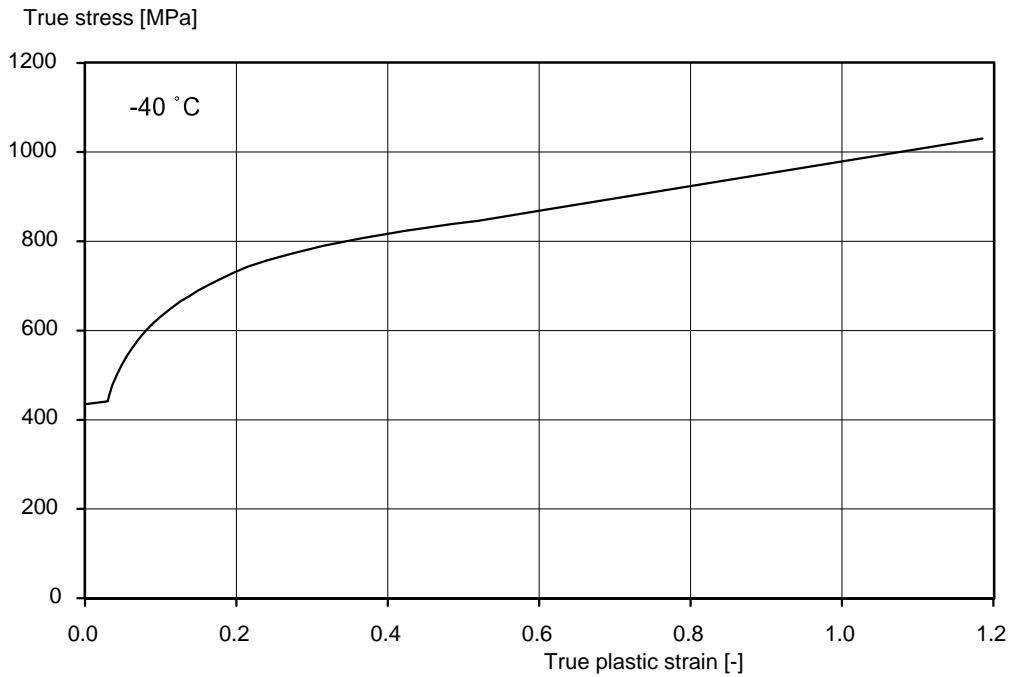


Figure 1 Material true-stress versus true-strain curve at -40 °C

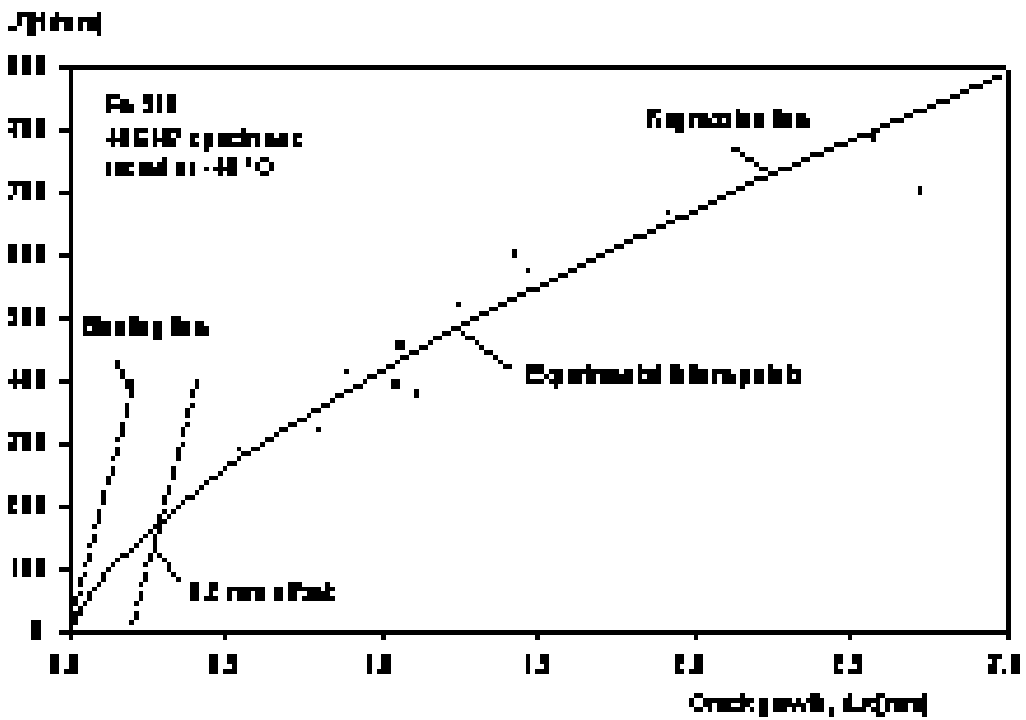


Figure 2 Fracture resistance curve of a Fe510 steel measured on side grooved 4-point single edge notched bend specimens tested at -40 °C

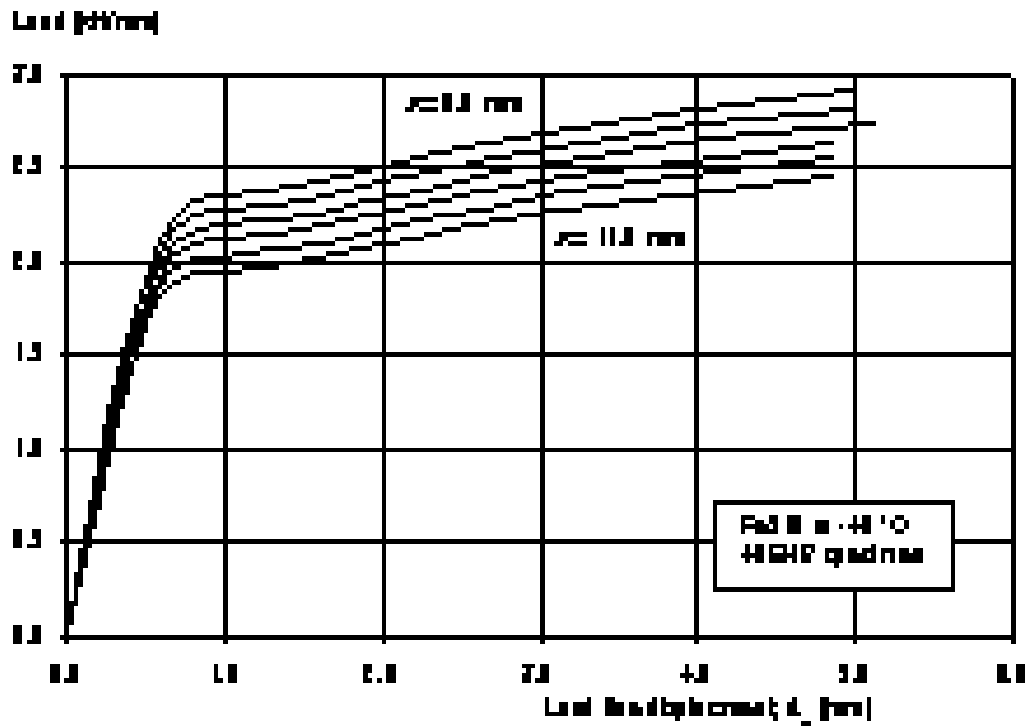


Figure 3
 Calculated load versus load line displacement as a function of crack length for the Fe510 steel 4SENB specimen tested at -40 °C. The crack length varied from $a = 9.0$ mm to 11.0 mm with steps of 0.2 mm. For convenience the results are plotted for $a = 9.0$ mm to 11.0 mm with steps of 0.4 mm

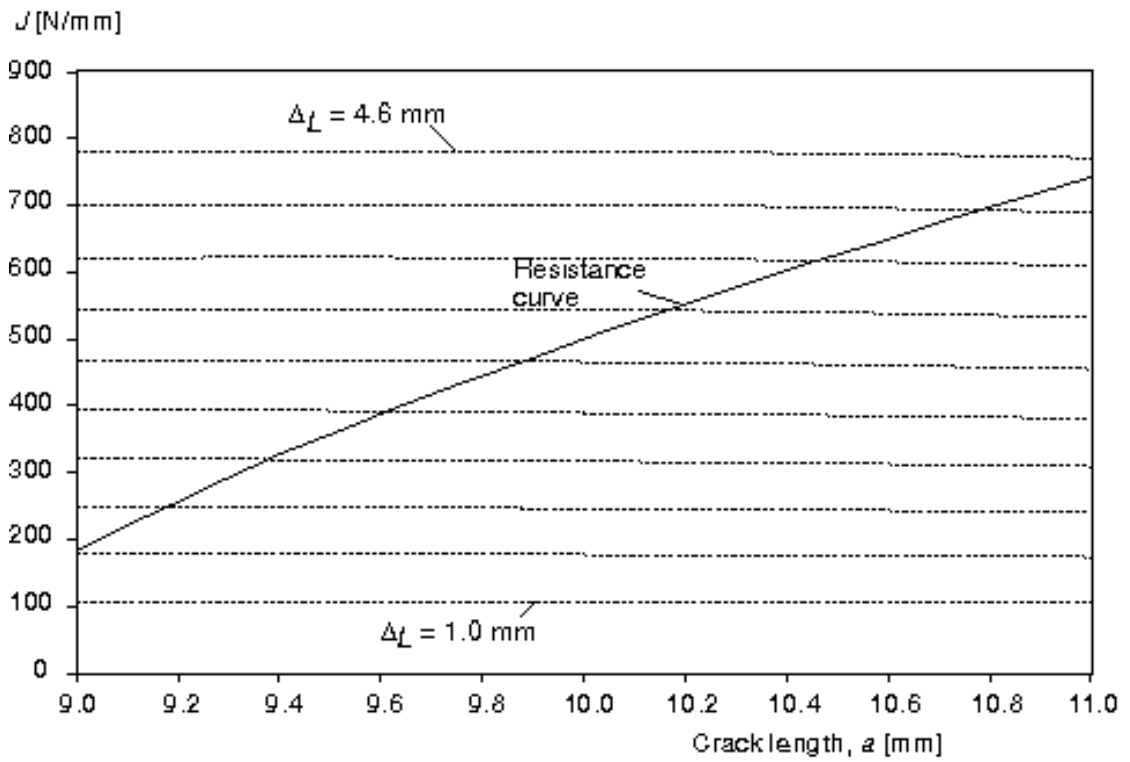


Figure 4
 Calculated constant load line displacement curves ($\Delta_L = 1.0, 1.4, \dots, 4.2, 4.6$ mm) as a function of J and Δa with the measured fracture resistance curve

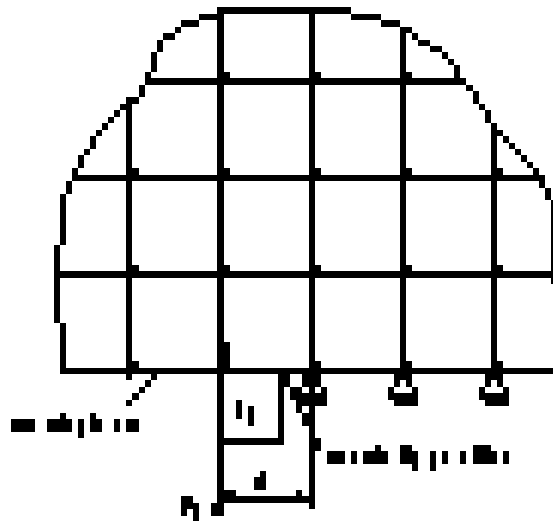


Figure 5 Node relaxation technique

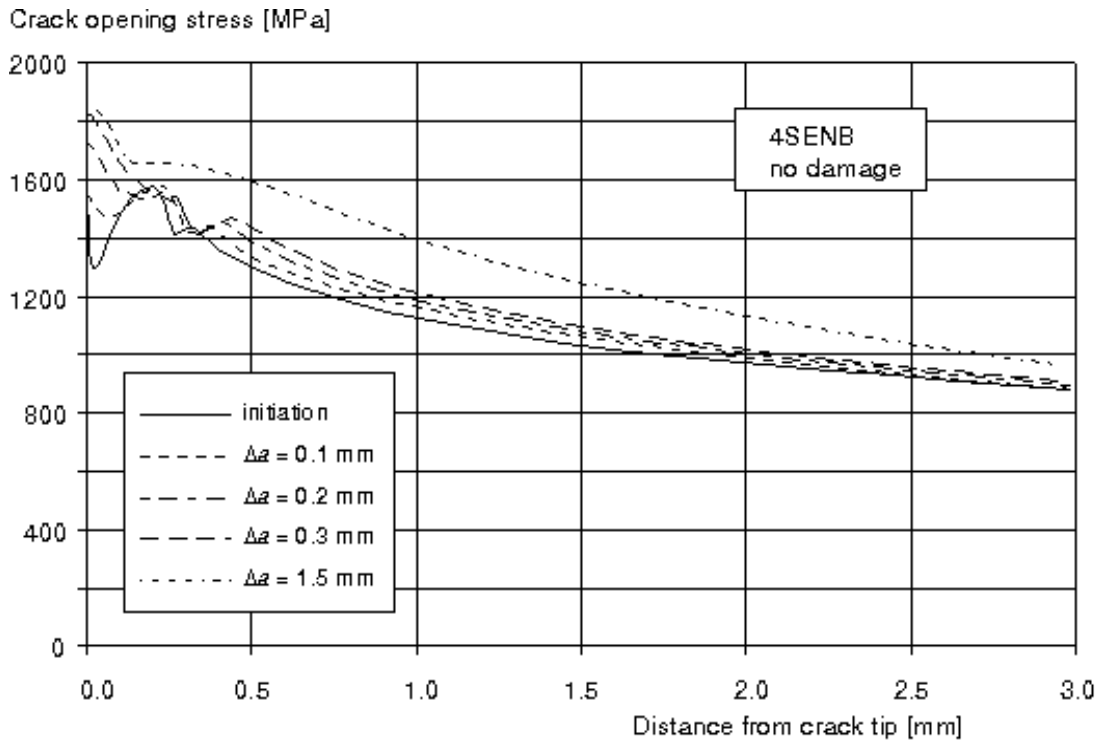


Figure 6
 Calculated stress distribution ahead of the growing crack in the 4SENB specimen based on the von Mises flow criterion

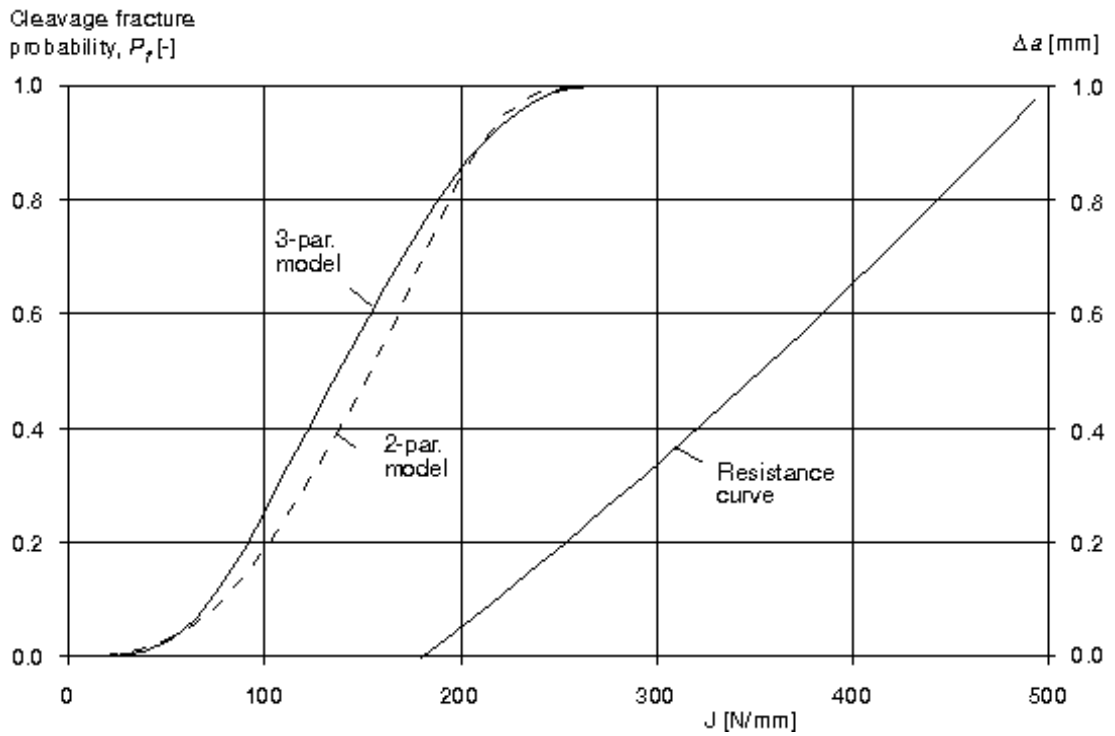


Figure 7
 Calculated probability of cleavage fracture and calculated resistance curve based on the von Mises flow criterion

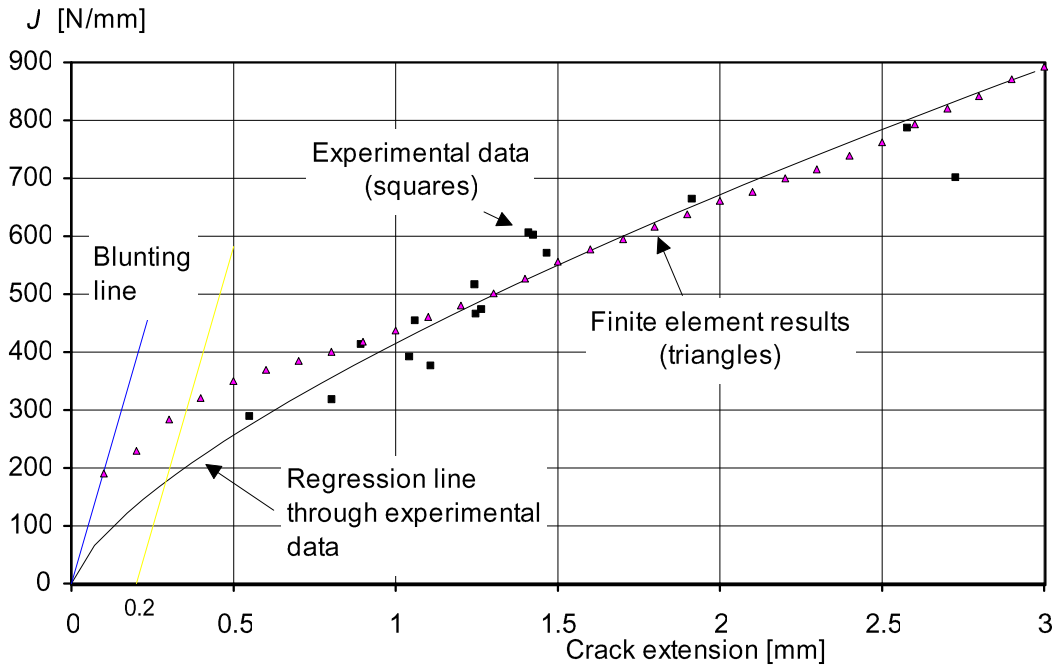


Figure 8 Damage analyses: Calculated fracture resistance curve and experimental data

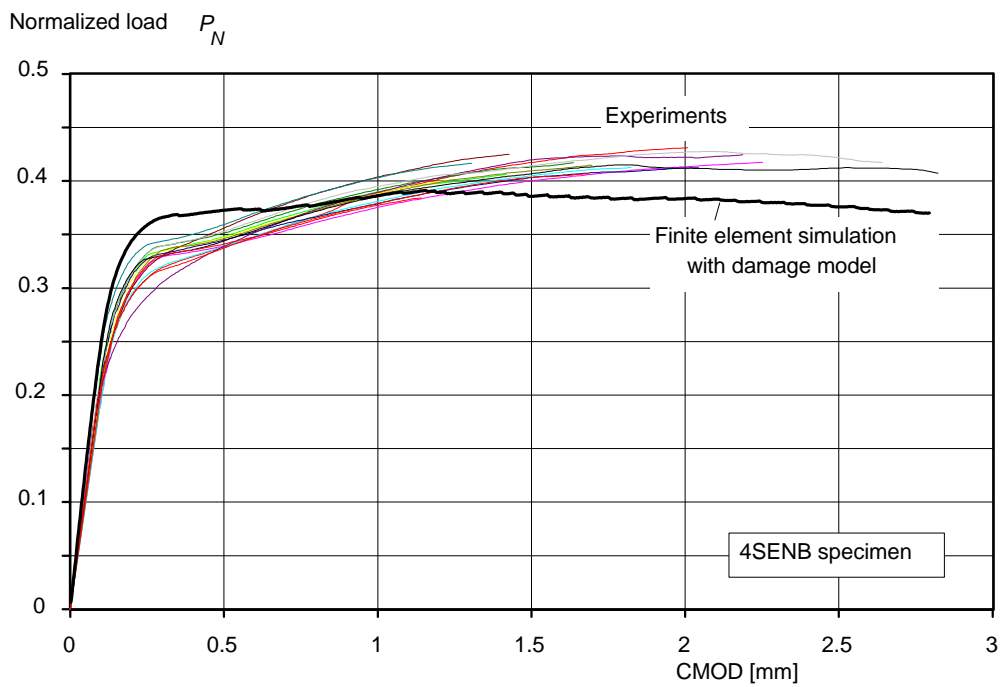


Figure 9 Damage analyses: Calculated load versus CMOD curves and experimental data

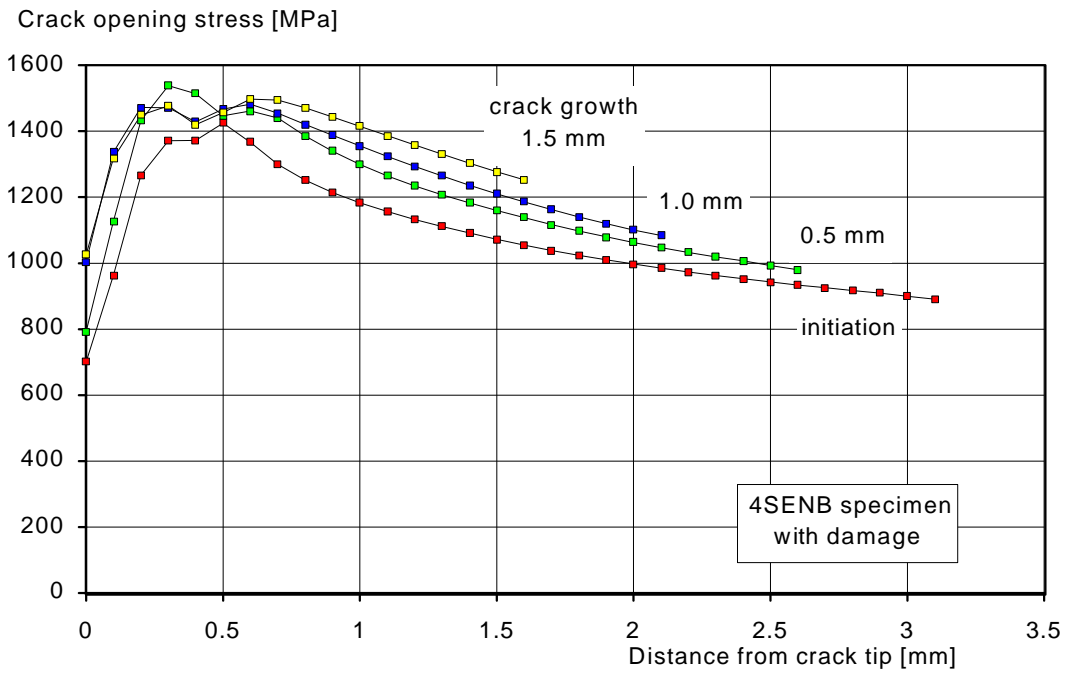


Figure 10

Damage analysis: Calculated crack opening stress ahead of the crack tip as a function of the amount of crack growth

Cleavage fracture probability [-]

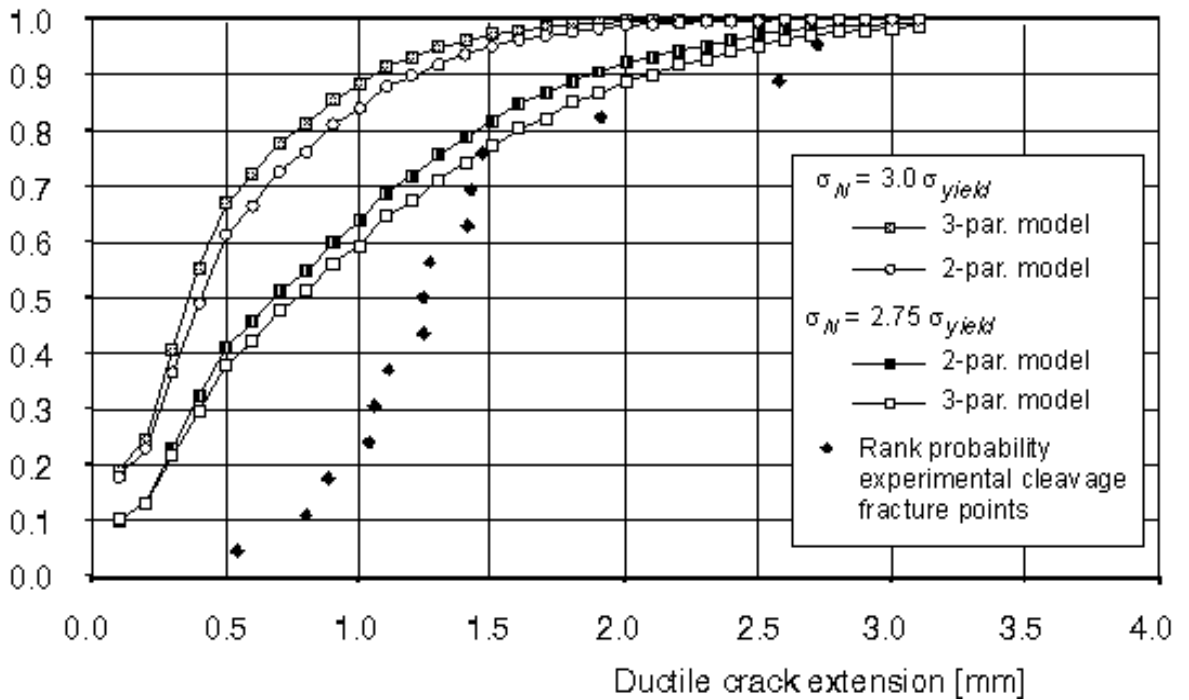


Figure 11

Damage analyses: Predicted cleavage fracture probability as a function of the prior amount of ductile tearing

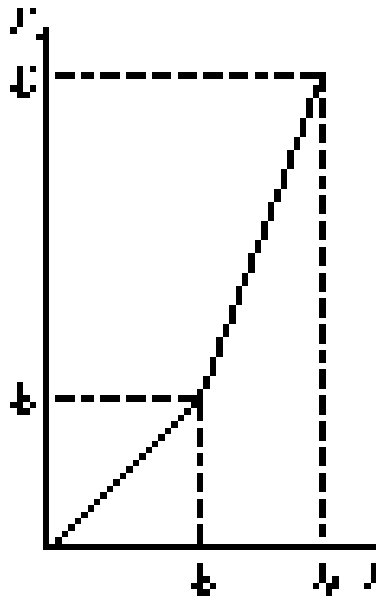


Figure I-2 Modified volume fraction

The rate of change of the void volume fraction is given by a nucleation and a growth contribution,

$$\dot{f} = \dot{f}_{growth} + \dot{f}_{nucleation} \tag{I.3}$$

with

$$\dot{f}_{growth} = (1-f) \dot{\epsilon}_{kk}^p \tag{I.4}$$

where $\dot{\epsilon}_{ij}^p$ represents the macroscopic plastic strain rate. Nucleation is shown to be given by the by the following equation

$$\dot{f}_{nucleation} = A \dot{\sigma}_M + B \dot{\sigma}_{kk}^p / 3. \tag{I.5}$$

Expressions for *A* and *B* will be given later on.

The equivalent tensile flow stress σ_M representing the actual microscopic stress state in the matrix material is related to the effective plastic microscopic strain state ϵ_M^p by the incremental relation

$$\dot{\sigma}_M = E^t \dot{\epsilon}_M^p \tag{I.6}$$

where E^t is the tangential slope in the uniaxial true stress-natural plastic strain curve at the current stress level σ_M .

1.1. Stress-strain relations

It will be assumed that the total strain rate is the sum of the elastic and plastic strain rate

$$\dot{\varepsilon}_{ij} = \dot{\varepsilon}_{ij}^e + \dot{\varepsilon}_{ij}^p \quad (\text{I.7})$$

Elasticity is given by Hooke's law

$$\dot{\sigma}_{ij} = E_{ijkl} \dot{\varepsilon}_{kl} \quad (\text{I.8})$$

The plastic part of the macroscopic strain rate is taken to be given by

$$\dot{\varepsilon}_{ij}^p = \Lambda \frac{\partial \phi}{\partial \sigma_{ij}} \quad (\text{I.9})$$

which implies macroscopic normality. It is furthermore assumed that this relation also holds during the nucleation of new voids.

The microscopic equivalent tensile flow stress σ_M and equivalent plastic strain ε_M^p are averages that do not specify the actual microscopic fields in the matrix material surrounding the voids. However, it is assumed that the rate of equivalent plastic work in the matrix material equals the macroscopic rate of plastic work,

$$\sigma_{ij} \dot{\varepsilon}_{ij}^p = (1-f) \sigma_M \dot{\varepsilon}_M^p \quad (\text{I.10})$$

Using the incremental work hardening relation (I.6) the rate of the equivalent flow stress in the matrix material is given by,

$$\dot{\sigma}_M = E_M^t \dot{\varepsilon}_M^p = E_M^t \frac{\sigma_{ij} \dot{\varepsilon}_{ij}^p}{(1-f) \sigma_M} \quad (\text{I.11})$$

Note that $\dot{\varepsilon}_M^p$ represent the effective strain of the matrix material and not the effective macroscopic plastic strain rate, $\dot{\varepsilon}^p$, defined by,

$$\dot{\varepsilon}^p = \sqrt{\frac{2}{3} \dot{\varepsilon}_{ij}^p \dot{\varepsilon}_{ij}^p} \quad (\text{I.12})$$

Plasticity occurs only if the yield function (I.1) is satisfied. Consistency requires that during plastic deformation the yield condition must be satisfied as well, resulting in

$$\dot{\phi} = \dot{\phi}(\sigma_{ij}, \sigma_M, f^*) = 0 \quad (\text{I.13})$$

or

$$\dot{\phi} = \frac{\partial \phi}{\partial \sigma_{ij}} \dot{\sigma}_{ij} + \frac{\partial \phi}{\partial \sigma_M} \dot{\sigma}_M + \frac{\partial \phi}{\partial f^*} \frac{df^*}{df} \dot{f} \quad (\text{I.14})$$

The first term represents the change due to changes in macroscopic stress. The second term represents the hardening effects in the matrix material, whereas the third term includes the contribution due to changes in void volume fraction.

1.2. Stress change effects

The contribution of the change in yield condition due to the change in stress results from a change in effective stress σ_e and a change in hydrostatic stress σ_{kk} is given by,

$$\frac{\partial \phi}{\partial \sigma_{ij}} = \frac{\partial \phi}{\partial \sigma_e} \frac{\partial \sigma_e}{\partial \sigma_{ij}} + \frac{\partial \phi}{\partial \sigma_{kk}} \frac{\partial \sigma_{kk}}{\partial \sigma_{ij}} \quad (\text{I.15})$$

It is now easily verified that the following relations hold

$$\frac{\partial \phi}{\partial \sigma_e} = \frac{2\sigma_e}{\partial \sigma_M^2} \quad (\text{I.16})$$

$$\frac{\partial \sigma_e}{\partial \sigma_{ij}} = \frac{3}{2} \frac{s_{ij}}{\sigma_e} \quad (\text{I.17})$$

$$\frac{\partial \phi}{\partial \sigma_{kk}} = f^* \frac{q_1 q_2}{\sigma_M} \sinh\left(\frac{q_2}{2} \frac{\sigma_{kk}}{\sigma_M}\right) \quad (\text{I.18})$$

$$\frac{\partial \sigma_{kk}}{\partial \sigma_{ij}} = \delta_{ij}. \quad (\text{I.19})$$

Substitution into equation (I.15) now gives

$$\frac{\partial \phi}{\partial \sigma_{ij}} = \frac{2}{\sigma_M} \left[\frac{3}{2} \frac{s_{ij}}{\sigma_M} + \frac{1}{2} f^* q_1 q_2 \sinh\left(\frac{q_2}{2} \frac{\sigma_{kk}}{\sigma_M}\right) \delta_{ij} \right] \quad (\text{I.20})$$

After introduction of the parameter α ,

$$\alpha = \frac{1}{2} f^* q_1 q_2 \sinh\left(\frac{q_2}{2} \frac{\sigma_{kk}}{\sigma_M}\right), \quad (\text{I.21})$$

and the normalised stress tensor m_{ij}^G ,

$$m_{ij}^G = \frac{3}{2} \frac{s_{ij}}{\sigma_M} + \alpha \delta_{ij}, \quad (\text{I.22})$$

equation (I.20) reduces to

$$\frac{\partial \phi}{\partial \sigma_{ij}} = \frac{2}{\sigma_M} m_{ij}^G. \quad (\text{I.23})$$

1.3. Hardening effects

The contribution to the yield condition due to changes in effective stress of the matrix material σ_M is accounted for in the following way

$$\frac{\partial \phi}{\partial \sigma_M} = -2 \frac{\sigma_e^{-3}}{\sigma_M^2} + 2 q_1 f^* \left(\frac{-q_2}{2} \frac{\sigma_{kk}}{\sigma_M} \right) \sinh\left(\frac{q_2}{2} \frac{\sigma_{kk}}{\sigma_M}\right). \quad (\text{I.24})$$

With the parameter α defined by equation (I.21), equation (I.24) reduces to

$$\frac{\partial \phi}{\partial \sigma_M} = -\frac{2}{\sigma_M} \left(\frac{\sigma_e^2}{\sigma_M^2} + \frac{\sigma_{kk}}{\sigma_M} \alpha \right) \quad (\text{I.25})$$

1.4 Void growth effects

The effect of change in volume fraction on the yield condition is determined by

$$\frac{\partial \phi}{\partial f^*} = 2 q_1 \cosh\left(\frac{q_2 \sigma_{kk}}{2 \sigma_M}\right) - 2 q_1^2 f^* \quad (\text{I.26})$$

After introduction of a parameter γ defined by

$$\gamma = q_1 \cosh\left(\frac{q_2 \sigma_{kk}}{2 \sigma_M}\right) - q_1^2 f^* \quad (\text{I.27})$$

equation (I.26) reduces to

$$\frac{\partial \phi}{\partial f^*} = 2\gamma \quad (\text{I.28})$$

It is also clear from equation (I.2) that f^* changes due to the rate of change of the void fraction f . Consequently

$$\begin{aligned} \frac{\partial f^*}{\partial f} &= 1 & \text{if } f \leq f_c \\ \frac{\partial f^*}{\partial f} &= \frac{f_u - f_c}{f_F - f_c} & \text{if } f > f_c \end{aligned} \quad (\text{I.29})$$

Using equations (I.3)-(I.5) and equation (I.11) the rate of change of the void fraction is now given by:

$$\begin{aligned} \dot{f} &= (1-f) \dot{\varepsilon}_{kk}^p + A \dot{\sigma}_M + \frac{B}{3} \dot{\sigma}_{kk} \\ &= (1-f) \dot{\varepsilon}_{kk}^p + \frac{A E^t \sigma_{ij}}{(1-f) \sigma_M} \dot{\varepsilon}_{ij}^p + \frac{B}{3} \dot{\sigma}_{kk} \end{aligned}$$

or

$$\dot{f} = \left[(1-f) \delta_{ij} + \frac{A E^t \sigma_{ij}}{(1-f) \sigma_M} \right] \dot{\varepsilon}_{ij}^p + \frac{B}{3} \dot{\sigma}_{kk} \quad (\text{I.30})$$

2. Incremental relation

Combination of equations (I.11), (I.30) and (I.9) with the consistency equation (I.14) gives

$$\begin{aligned} \dot{\phi} &= \frac{\partial \phi}{\partial \sigma_{ij}} \dot{\sigma}_{ij} + \frac{\partial \phi}{\partial \sigma_M} \frac{E^t \sigma_{ij}}{(1-f) \sigma_M} \Lambda \frac{\partial \phi}{\partial \sigma_{ij}} + \\ &+ \frac{\partial \phi}{\partial f^*} \frac{df^*}{df} \left[\frac{B}{3} \dot{\sigma}_{ij} \delta_{ij} + \left((1-f) \delta_{ij} + \frac{A E^t \sigma_{ij}}{(1-f) \sigma_M} \right) \Lambda \frac{\partial \phi}{\partial \sigma_{ij}} \right] = 0 \end{aligned} \quad (\text{I.31})$$

After introduction of a scalar hardening factor H defined by

$$H = -(1-f) \frac{\partial \phi}{\partial f^*} \frac{df^*}{df} \frac{\partial \phi}{\partial \sigma_{ij}} \delta_{ij} - \left(\frac{\partial \phi}{\partial f^*} \frac{df^*}{df} A + \frac{\partial \phi}{\partial \sigma_M} \right) \frac{E^t \sigma_{ij}}{(1-f) \sigma_M} \frac{\partial \phi}{\partial \sigma_{ij}} \quad (\text{I.32})$$

the consistency equation reduces to

$$\left(\frac{\partial \phi}{\partial \sigma_{ij}} + \frac{\partial \phi}{\partial f^*} \frac{df^*}{df} \frac{B}{3} \delta_{ij} \right) \dot{\sigma}_{ij} - \Lambda H = 0. \quad (\text{I.33})$$

With (I.28) and (I.20) the term between brackets in (I.33) can be evaluated

$$\left(\frac{\partial \phi}{\partial \sigma_{ij}} + \frac{\partial \phi}{\partial f^*} \frac{df^*}{df} \frac{B}{3} \delta_{ij} \right) = \frac{2}{\sigma_M} \left(\frac{3}{2} \frac{S_{ij}}{\sigma_M} + \alpha \delta_{ij} + \gamma \frac{df^*}{df} \frac{B}{3} \sigma_M \delta_{ij} \right); \quad (\text{I.34})$$

Next we introduce the scalar parameter β

$$\beta = \alpha + \gamma \frac{df^*}{df} \frac{B}{3} \quad (\text{I.35})$$

and a normalised stress tensor m_{ij}^F (different from m_{ij}^G in equation (I.22))

$$m_{ij}^F = \frac{3}{2} \frac{S_{ij}}{\sigma_M} + \beta \delta_{ij} \quad (\text{I.36})$$

The consistency equation (I.33) then reads

$$\frac{2}{\sigma_M} m_{ij}^F \dot{\sigma}_{ij} - \Lambda H = 0. \quad (\text{I.37})$$

Using equations (I.37) and (I.23) the macroscopic plastic strain rate (I.9) is given by

$$\dot{\epsilon}_{ij}^p = \Lambda \frac{\partial \phi}{\partial \sigma_{ij}} = \frac{1}{H} \frac{2}{\sigma_M} m_{kl}^F \dot{\sigma}_{kl} = \frac{2}{\sigma_M} m_{ij}^G \dot{\sigma}_{ij}. \quad (\text{I.38})$$

Note that the macroscopic plastic strain rate only has a value if the yield condition is satisfied and

$$\frac{1}{H} \frac{2}{\sigma_M} m_{ij}^F \dot{\sigma}_{ij} > 0. \quad (\text{I.39})$$

Finally the elasticity relation is used to obtain the stress rate - strain rate equation

$$\begin{aligned} \dot{\sigma}_{ij} &= E_{ijkl} \left(\dot{\epsilon}_{kl} - \dot{\epsilon}_{kl}^p \right) \\ &= E_{ijkl} \dot{\epsilon}_{kl} - E_{ijkl} \Lambda \frac{\partial \phi}{\partial \sigma_{kl}} \end{aligned} \quad (\text{I.40})$$

Pre-multiplication with $\frac{2}{\sigma_M} m_{ij}^F$ and combination with equation (I.38) determines the scalar Λ ,

$$\Lambda = \frac{\frac{2}{\sigma_M} m_{ij}^F E_{ijkl} \dot{\epsilon}_{kl}}{\frac{4}{2} m_{pq}^F E_{pqrs} m_{rs}^G + H} \quad (I.41)$$

At this stage it is convenient to introduce another parameter λ such that the macroscopic plastic strain rate is given by

$$\dot{\epsilon}_{ij}^p = \Lambda \frac{\partial \phi}{\partial \sigma_{ij}} = \Lambda \frac{2}{\sigma_M} m_{ij}^G = \lambda m_{ij}^G$$

thus

$$\lambda = \frac{2}{\sigma_M} \Lambda \quad (I.42)$$

Note that λ as well as m_{ij}^G are dimensionless, whereas Λ and $\frac{\partial \phi}{\partial \sigma_{ij}}$ have the dimension of stress and stress⁻¹ respectively.

In addition we introduce another hardening parameter h defined by

$$H = \frac{4}{2} \frac{h}{\sigma_M} \quad (I.43)$$

The scalar factor λ is now given by

$$\lambda = \frac{m_{ij}^F E_{ijkl} \dot{\epsilon}_{kl}}{m_{pq}^F E_{pqrs} m_{rs}^G + h} \quad (I.44)$$

Substitution of equations (I.43) and (I.41) into equation (I.40) then gives

$$\dot{\sigma}_{ij} = (E_{ijkl} - Y_{ijkl}) \dot{\epsilon}_{kl} \quad (I.45)$$

where the plasticity tensor Y_{ijkl} is defined by

$$Y_{ijkl} = \frac{E_{ijmn} m_{mn}^G m_{pq}^F E_{pqkl}}{m_{ab}^F E_{abcd} m_{cd}^G + h} \quad (I.46)$$

The hardening factor H as defined in (I.32) can be rewritten using equations (I.23), (I.25) and (I.28)

$$H = -(1-f) 2 \gamma \frac{df^*}{df} \frac{2}{\sigma_M} m_{ij}^G \delta_{ij} - \left[2 \gamma \frac{df^*}{df} A - \frac{2}{\sigma_M} \left(\frac{\sigma_e^2}{2} + \frac{\sigma_{kk}}{\sigma_M} \alpha \right) \right] \frac{E^t}{(1-f) \sigma_M} \sigma_{ij} \frac{2}{\sigma_M} m_{ij}^G \quad (I.47)$$

Using the definition of m_{ij}^G equation (I.22) it can now be shown that

$$\frac{1}{\sigma_M} \sigma_{ij} m_{ij}^G = \frac{\sigma_e^2}{\sigma_M^2} + \frac{\sigma_{kk}}{\sigma_M} \alpha \quad (I.48)$$

$$m_{ij}^G \delta_{ij} = 3\alpha \quad (I.49)$$

The hardening factor then results in

$$H = \frac{4}{\sigma_M^2} \left[\frac{E^t}{(1-f)} \left(\frac{\sigma_e^2}{\sigma_M^2} + \frac{\sigma_{kk}}{\sigma_M} \alpha \right)^2 - \frac{E^t}{(1-f)} \gamma A \sigma_M \frac{df^*}{df} \left(\frac{\sigma_e^2}{\sigma_M^2} + \frac{\sigma_{kk}}{\sigma_M} \alpha \right) - (1-f) \sigma_M \gamma \frac{df^*}{df} 3\alpha \right]$$

or

$$h = \frac{E^t}{(1-f)} \left(\frac{\sigma_e^2}{\sigma_M^2} + \frac{\sigma_{kk}}{\sigma_M} \alpha \right)^2 - \sigma_M \gamma \frac{df^*}{df} \left[3\alpha (1-f) + \frac{E^t}{(1-f)} A \left(\frac{\sigma_e^2}{\sigma_M^2} + \frac{\sigma_{kk}}{\sigma_M} \alpha \right) \right] \quad (I.50)$$

Note:

for a von Mises material, (obtained with $f^* = 0$ and as a consequence $\alpha = 0$; $\gamma = 0$), equation (I.50) reduces to $h = E^t$ and thus the classical set of elastic - plastic relations is obtained.

The hardening slope E^t is defined as the slope of the true stress - effective plastic strain curve of the matrix material. The matrix material quantities σ_M and $\dot{\epsilon}_M^p$ are related to the macroscopic quantities σ_{ij} and $\dot{\epsilon}_{ij}^p$ by the incremental work hardening relation (I.10). The change in effective plastic strain $\dot{\epsilon}_M^p$ can now be obtained using the normality law

$$\dot{\epsilon}_M^p = \frac{1}{(1-f)} \frac{\sigma_{ij} \dot{\epsilon}_{ij}^p}{\sigma_M} = \frac{\lambda}{(1-f)} \frac{1}{\sigma_M} m_{ij}^G \sigma_{ij}$$

or, with equation (I.48)

$$\dot{\epsilon}_M^p = \frac{\lambda}{(1-f)} \left(\frac{\sigma_e^2}{\sigma_M^2} + \frac{\sigma_{kk}}{\sigma_M} \alpha \right) \quad (I.51)$$

and thus is the change in effective stress given by

$$\dot{\sigma}_M = \frac{E^t \lambda}{(1-f)} \left(\frac{\sigma_e^2}{\sigma_M^2} + \frac{\sigma_{kk}}{\sigma_M} \alpha \right) \quad (I.52)$$

Note that the macroscopic effective plastic strain rate as defined by equation (I.12) can be evaluated as

$$\dot{\bar{\epsilon}}^p = \lambda \sqrt{\left(\frac{\sigma_e}{\sigma_M}\right)^2 + 2\alpha^2} . \quad (\text{I.53})$$

Hence only if the void fraction f equals zero both quantities $\dot{\epsilon}_M^p$ and $\dot{\bar{\epsilon}}^p$ are identical.

Summarising:

The incremental stress- strain relation, based on a known value of stress σ_{ij} , macroscopic strains ϵ_{ij} and ϵ_{ij}^p a set of parameters characterising the material state: volume fraction f , effective plastic strain ϵ_M^p and effective stress σ_M , can be written in the following form

$$\begin{aligned} \dot{\sigma}_{ij} &= (E_{ijkl} - Y_{ijkl}) \dot{\epsilon}_{kl} \\ Y_{ijkl} &= \frac{E_{ijmn} m_{mn}^G m_{pq}^F E_{pqkl}}{m_{ab} E_{abcd} m_{cd} + h} \\ h &= \frac{E^t}{(1-f)} \left(\frac{\sigma_e^2}{\sigma_M^2} + \frac{\sigma_{kk}}{\sigma_M} \alpha \right)^2 + \\ &\quad - \sigma_M \gamma \frac{df^*}{df} \left[3\alpha(1-f) + \frac{E^t}{(1-f)} A \left(\frac{\sigma_e^2}{\sigma_M^2} + \frac{\sigma_{kk}}{\sigma_M} \alpha \right) \right] \end{aligned}$$

with

$$\begin{aligned} m_{ij}^G &= \frac{3}{2} \frac{S_{ij}}{\sigma_M} + \alpha \delta_{ij} \\ m_{ij}^F &= \frac{3}{2} \frac{S_{ij}}{\sigma_M} + \beta \delta_{ij} \\ \alpha &= \frac{1}{2} f^* q_1 q_2 \sinh\left(\frac{q_2 \sigma_{kk}}{2 \sigma_M}\right) \\ \beta &= \alpha + \gamma \frac{df^*}{df} \frac{B}{3} \\ \gamma &= q_1 \cosh\left(\frac{q_2 \sigma_{kk}}{2 \sigma_M}\right) - q_1^2 f^* \end{aligned}$$

Having obtained a value for the total strain rate, a scalar factor λ is defined by

$$\lambda = \frac{m_{ij}^F E_{ijkl} \dot{\epsilon}_{kl}}{m_{pq}^F E_{pqrs} m_{rs}^G + h}$$

and the changes in effective strain and stress is:

$$\dot{\epsilon}_M^p = \frac{\lambda}{(1-f)} \left(\frac{\sigma_e^2}{\sigma_M^2} + \frac{\sigma_{kk}}{\sigma_M} \alpha \right)$$

$$\dot{\sigma}_M = E^t \dot{\epsilon}_M^p$$

The plastic strain components $\dot{\epsilon}_{ij}^p$ are given by

$$\dot{\epsilon}_{ij}^p = \lambda m_{ij}^G$$

Thus a complete set of incremental relations has been obtained. Note that the yield tensor Y_{ijkl} is only symmetric of $B = 0$.

3. Void nucleation and void growth

The rate of change of the void volume fraction is given by equation (I.3) and consists of a growth part and a nucleation part. The growth rate is defined by the volumetric plastic strain rate

$$\dot{\epsilon}_{kk}^p = \lambda m_{ij}^G \delta_{ij} = 3 \alpha \lambda \quad (\text{I.54})$$

and thus the growth rate is given by

$$\dot{f}_{growth} = (1-f) 3 \alpha \lambda \quad (\text{I.55})$$

The nucleation rate in equation (I.5) could be defined by:

$$\dot{f}_{nucleation} = A \dot{\sigma}_M + B \frac{\dot{\sigma}_{kk}}{3} \quad (\text{I.56})$$

For stress controlled nucleation $A = B$ are given by,

$$A = B = \frac{f_{N\sigma}}{s_\sigma \sqrt{2\pi}} \exp \left[-\frac{1}{2} \left\{ \frac{\left(\sigma_M + \frac{\sigma_{kk}}{3} \right) - \sigma_N}{s_\sigma} \right\}^2 \right] \quad (\text{I.57})$$

$$\text{for } \sigma_M + \frac{\sigma_{kk}}{3} = \left(\sigma_M + \frac{\sigma_{kk}}{3} \right)_{\max} \text{ and } \left(\dot{\sigma}_M + \frac{\dot{\sigma}_{kk}}{3} \right) > 0$$

where σ_N is the mean maximum stress for nucleation and s_σ the standard deviation of the stress over which most of the voids nucleate $f_{N\sigma}$ is the volume fraction of the *stress* controlled void nucleating particles.

In case nucleation is *strain* controlled the parameters A and B are defined by,

$$A = \frac{1}{E^t} \frac{f_{N\varepsilon}}{s_\varepsilon \sqrt{2\pi}} \exp \left[-\frac{1}{2} \left(\frac{\varepsilon_M^p - \varepsilon_N}{s_\varepsilon} \right)^2 \right] \quad (I.58)$$

$$B = 0 \quad \text{for } \varepsilon_M^p = (\varepsilon_M^p)_{\max} \text{ and } \dot{\varepsilon}_M^p > 0$$

where ε_N is the mean equivalent plastic strain at which nucleation occurs, s_ε is the corresponding standard deviation of the equivalent plastic strain and $f_{N\varepsilon}$ is the volume fraction of *strain* controlled void nucleating particles.

Other nucleation mechanisms can be introduced by modifying the parameters A and B .

4. Generalisation to large strains

The set of equations discussed in the previous sections were derived based on small strain theory. Similar to the generalisation of the small strain relations for a material with a von Mises yield function as done by TVERGAARD [20], NAGTEGAAL and DE JONG [21], the transformations required to obtain a formulation suitable for large strains are straight forward. The stress rate terms are now replaced by the Jaumann rate of stress defined by

$$\dot{\sigma}_{ij}^J = \dot{\sigma}_{ij} + (\delta_{ik} \sigma_{jl} + \delta_{jk} \sigma_{il}) \dot{\varepsilon}_{kl} \quad (I.59)$$

We now have the stress-strain relation

$$\dot{\sigma}_{ij}^J = (R_{ijkl} - Y_{ijkl}) \dot{\varepsilon}_{kl} \quad (I.60)$$

with

$$R_{ijkl} = E_{ijkl} - \frac{1}{2} (\sigma_{ik} \delta_{jl} + \sigma_{jk} \delta_{il} + \sigma_{il} \delta_{jk} + \sigma_{jl} \delta_{ik}) + \sigma_{ij} \delta_{kl}. \quad (I.61)$$

In standard von Mises plasticity with small elastic strains the last term in equation (I.61) can be neglected since it is related to the volumetric strain. In view of the volumetric strains for large volume fractions (as can be seen from equation (I.54)) this term can not be neglected here. The last term will result in a non-symmetry of the moduli. For stress controlled nucleation mechanisms ($B \neq 0$) clearly non-symmetry of Y_{ijkl} was observed.

References

1. van Rongen, H.J.M., *Proceedings of the 8th International Conference on Offshore Mechanics and Arctic Engineering (OMAE-8)*, (Edited by M.M. Salama et al.), ASME, New York, 665-673.
2. Bakker, A. and Koers, R.W.J., "Prediction of cleavage fracture events in the brittle-ductile transition region of a ferritic steel", *Defect Assessment in Components - Fundamentals and Applications*, ESIS/EGF9 (Edited by J.G. Blauel and H.-H. Schwalbe), Mechanical Engineering Publications, London, 1991, pp 613-632.
3. Bakker, A., "Influence of material flow curve modelling on fracture mechanics evaluations", *Numerical methods in Fracture Mechanics: Proceedings of the Fifth Int. Conf. held in Freiburg (FRG)*, (Edited by A.R. Luxmoore and D.R.J. Owen, 1990, pp 443-449.
4. Beremin, F.M.: "A local Criterion for Cleavage Fracture of a Nuclear Pressure Vessel Steel", *Met. Trans*, Vol. 14A, 1983, pp 2277-2287.
5. Wallin, K., Saario, T. and Törrönen, K.: "Statistical model for carbide induced fracture in steel", *Metal Science*, 1984, Vol. 18, pp 13-16.
6. Knott, J.F., "Micro mechanisms of fracture - The role of micro mechanisms", *ECF9: Reliability and structural integrity of advanced materials*, (Editors Sedmak S. et. al.), Varna, Bulgaria, 1992, pp 1375-1400.
7. Peeters, F.J.H. and Koers, R.W.J., "Numerical simulation of dynamic crack propagation phenomena by means of the finite element method", *Fracture control of engineering structures - ECF6*, (Editors H.C. van Elst and A. Bakker), Amsterdam June 15-20, 1986, Vol. III, pp 2205-2224.
8. McMeeking, R.M.: "Finite deformation analysis of crack-tip opening in elastic-plastic materials and implications for fracture", *J. Mech. Phys. Solids*, 1977, Vol. 25, pp 357-381.
9. Varias, A.G. and Shih, C.F.: "Quasi-static crack advance under a range of constraints - steady-state fields based on a characteristic length.", *J. Mech. Phys. Solids*, 1993, Vol. 41, No. 5, pp 835-861.
10. Berg, C.A., "Plastic Dilatation and Void Interaction", *Proc. of the Batelle memorial Institute Symposium on Inelastic Processes in Solids*, 1969, pp 171-209.
11. Gurson, A.L., "Plastic flow and fracture behaviour of ductile materials incorporating void nucleation, growth and interaction", *Thesis Brown University*, 1975.
12. Gurson, A.L., "Continuum theory of ductile rupture by void nucleation and growth; Part 1 - Yield criteria and flow rules for porous ductile media", *Trans. ASME, Ser. H*, Vol. 99, 1977, pp 2-15.
13. Tvergaard, V., "Influence of voids on shear band instabilities under plane strain conditions", *Int. J. of Fracture*, Vol. 17, 1981, pp 389-407.
14. Tvergaard, V. and Needleman, A., "Analysis of the cup-cone fracture in a round tensile bar", *Acta Metallurgica*, 1984, Vol. 32, pp 157-169.
15. Chu, C.C. and Needleman, A., "Void Nucleation Effects in Biaxially Stretched Sheets", *Trans. of the ASME: J. of Engineering Materials and Technology*, 1980, Vol. 102, pp 249-256.
16. Needleman, A. and Rice, J.R., "Limits to Ductile Set by Plastic Flow Localization", *Mechanics of Sheet Metal Forming*, Plenum Press, New York, 1978, pp 237.
17. Goods, S.H. and Brown, L.M., "The nucleation of cavities by plastic deformation", *Acta Metallurgica*, 1979, Vol. 27, pp 1-15.
18. MARC version K5.2, *General purpose finite element computer program*.

References (Cont'd)

19. Koplik, J. and Needleman, A., "Void growth and coalescence in porous plastic solids", *Int. J. Solids Structures*, Vol. 24, No. 8, 1988, pp 835-853.
20. Tvergaard, V, "Material failure by void growth to coalescence", *Report S 45 - Technical university of Denmark*, 1988.
21. Nagtegaal, J.C. and de Jong, J.E., "Some computational aspects of elastic-plastic large strain analysis, *Int. J. Num. Methods in Eng.*,1981 , **17**, p.15